Hydration Kinetics and Microstructure Development of Normal and $CaCl_2$-Accelerated Tricalcium Silicate Pastes

Jeffrey J. Thomas,*,† Andrew J. Allen,‡ and Hamlin M. Jennings§

Department of Civil and Environmental Engineering, Northwestern University, Evanston, Illinois 60208, Materials Science and Engineering Laboratory, National Institute of Standards and Technology, Gaithersburg, Maryland 20899, and Department of Materials Science and Engineering, Northwestern University, Evanston, Illinois 60208

Received: July 24, 2009; Revised Manuscript Received: October 7, 2009

Microstructure development and the kinetics of hydration of pure tricalcium silicate (C_3S) and $CaCl_2$-accelerated C_3S pastes were investigated by performing isothermal calorimetry and in situ small-angle neutron scattering (SANS) measurements on parallel specimens during the first few days of hydration, as well as on 28-day old specimens hydrated under the same curing conditions (water/cement ratio = 0.5, 20 °C). Calorimetry experiments were also performed over a range of hydration temperatures from 10 to 40 °C. The calorimetry data were analyzed by applying a previously described boundary nucleation and growth model. The model indicates that $CaCl_2$ significantly increases the rate of nucleation of hydration product on the surface of the C_3S particles but has relatively little effect on the product growth rate. The SANS measurements indicate that the composition and density of the calcium−silicate−hydrate (C−S−H) nanoparticles is unchanged by the addition of $CaCl_2$. However, in the $CaCl_2$-accelerated paste the surface fractal scattering associated with the deposition of hydration product onto the initially smooth surfaces of the C_3S particles rapidly declines in intensity and essentially disappears by the age of 1 day, while in the pure C_3S paste the surface fractal scattering remains prominent throughout the hydration process. The key observations from both the calorimetry and SANS analysis can be explained if in a pure C_3S paste the C−S−H hydration product forms initially with a low packing density and then densifies at later times.

Introduction

In this study, the early hydration of tricalcium silicate (C_3S), the main mineral in portland cement, is studied using isothermal calorimetry and small-angle neutron scattering (SANS). Isothermal calorimetry is the most accurate method of measuring the overall rate of hydration as a function of time, and recent advances in interpreting the calorimetry data in terms of a nucleation and growth process[1,2] allow a significant amount of information about the reaction process to be obtained from mathematical fits to the data. SANS is a powerful technique for characterizing the micro- and nanostructures of disordered materials such as hydrated cementitious materials.[3,4] It has the additional important advantages of working well on water-saturated materials and (given sufficient neutron flux) being rapid enough to monitor the early hydration process of a specimen in real time. By performing the calorimetry and SANS measurements on parallel paste specimens hydrated at the same temperature, the results can be combined to generate new insights into the relationships between the hydration kinetics and microstructure development.

An important variable investigated here is the effect on cement hydration of adding calcium chloride ($CaCl_2$), a powerful and widely used accelerator of C_3S and portland cement. Typically added in the amount of 1−2% by mass of cement, $CaCl_2$ significantly reduces the time to set and increases the short-term strength. The long-term strength is not increased, however, and the use of $CaCl_2$ has well-known disadvantages including an increased susceptibility to drying shrinkage and corrosion of steel reinforcement due to high chloride concentrations in the pore solution. Nevertheless, $CaCl_2$ is, with the possible exception of sucrose, the most widely studied chemical admixture for cement. It is well established that $CaCl_2$ acts by accelerating the rate of hydration of C_3S.[5] While the mechanism for the increased rate of hydration and the specific changes to the microstructure of the hydration products in the presence of $CaCl_2$ are not fully understood, the effects are generally thought to be related to its ability to flocculate hydrophilic colloids such as calcium−silicate−hydrate (C−S−H) gel, the main hydration product.[6,7]

Experimental Section

Two batches of triclinic C_3S powder were used in the experiments reported here, denoted batches 1 and 2. Batch 1 was provided courtesy of the Lafarge Research Center in Lyon, France, while batch 2 was obtained from Construction Technology Laboratories (Skokie, IL). (Certain commercial materials and equipment are identified in this paper only to specify adequately the experimental procedure. In no case does such identification imply recommendation by NIST nor does it imply that the material or equipment identified is necessarily the best available for this purpose.) As measured by SANS, the surface areas of these powders, with their estimated standard deviation uncertainties, are (0.71 ± 0.04) m^2/g for batch 1 and (0.47 ± 0.03) m^2/g for batch 2. Throughout this paper all estimated or

* To whom correspondence should be addressed. E-mail: jthomas@northwestern.edu.
† Department of Civil and Environmental Engineering, Northwestern University.
‡ National Institute of Standards and Technology.
§ Departments of Civil and Environmental Engineering and Materials Science and Engineering, Northwestern University.

10.1021/jp907078u CCC: $40.75
Published on Web 10/26/2009

computed uncertainties quoted are one-sigma standard deviations. For all of the experiments reported here, the C_3S was mixed by hand for 2 min at a water-to-cement mass ratio of 0.5, using either deionized water (control pastes) or a 4% mass aqueous solution of $CaCl_2$ (accelerated pastes). The latter mix design resulted in a 2% mass addition of $CaCl_2$ with respect to the mass of C_3S.

For the isothermal calorimetry experiments, about 1 g of paste was tightly sealed inside a 1.3-mL glass ampule before being placed into the calorimeter (Model 4200, Calorimetry Sciences Corporation, Linden, UT). This instrument has a sensitivity to heat input or output of 0.4 μJ and a baseline stability of 0.08 μW h^{-1}. Accelerated and control pastes made from both batches of C_3S were measured at 20 °C. For batch 2 only, experiments were conducted at temperatures ranging from 10 to 40 °C to measure the temperature dependence of the kinetic parameters.

The SANS experiments were performed using the 30 m NG7 SANS instrument[8] at the NIST Center for Neutron Research (NCNR) in Gaithersburg, MD, using a neutron wavelength, λ, of 0.8 nm. Accelerated and control pastes made from batch 1 C_3S were mixed at the same time and then sealed into quartz sample cells with an inside thickness (neutron path length) of 1 mm. The specimen temperatures were maintained at 20 °C, allowing direct comparison with the 20 °C calorimetry data. SANS measurements were performed regularly over the first 40 h of hydration. For each measurement, data were taken using three sample-to-detector distance configurations, giving an effective q-range (where q is the magnitude of the scattering vector, such that $q = (4\pi/\lambda) \sin \theta$ and θ is half the scattering angle) of 0.02−2.2 nm^{-1}. The average time between measurements on each paste was about 1.5 h. In addition, accelerated and control pastes were prepared 28 days prior to the SANS experiment following the same protocol and stored in sealed containers at room temperature. A few days before the experiment these pastes were cut into thin coupons suitable for SANS analysis. These specimens provide an indication of the microstructural changes that occur between 2 and 28 days of hydration.

Results

Analysis of Hydration Kinetics Determined by Calorimetry. The isothermal calorimetry data are shown in Figure 1. The rate data in the main plot are the measured data from the instrument, normalized to the mass of C_3S in the paste, while the cumulative heat data shown in the inset plot were obtained by integrating the rate data. The significant accelerating effects of $CaCl_2$ are clearly evident as an earlier and much higher rate peak and a near doubling of the evolved heat at any given time during the first two days of hydration. These differences can be quantified by applying a mathematical nucleation and growth model to the kinetic data.

It is now fairly well recognized[1,5,9] that application of the Avrami nucleation and growth equation to C_3S hydration is fundamentally problematic because the underlying assumption that nuclei are randomly distributed throughout the transforming volume conflicts with the observation that nucleation only occurs close to the particle surfaces. Recently, one of the authors[1] showed that a mathematical model for the kinetics of a solid-state transformation initiated at grain boundaries[10] can be adapted to provide a better physical description of the C_3S hydration process. The boundary nucleation equations describe a process for which continuous heterogeneous nucleation occurs on randomly distributed internal boundaries (corresponding to the C_3S particle surfaces), and the rate of growth of the nucleated

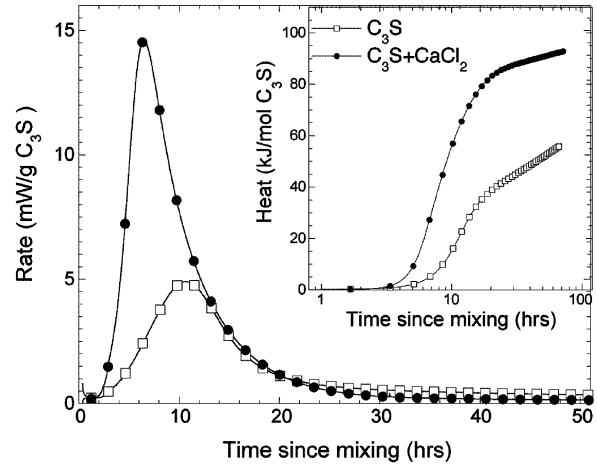

Figure 1. Early hydration kinetics of pure C_3S paste (open squares) and $CaCl_2$-accelerated C_3S paste (solid circles) as measured by isothermal calorimetry at 20 °C. The main plot shows the rate of heat evolution, and the inset shows the cumulative heat evolved. The lines are the data and the symbols, which are larger than the experimental uncertainties, are used only to identify the data sets.

regions of the transformed phase (i.e., hydration product) in all directions is constant with time. The transformed volume fraction X at time t for this type of process is[10]

$$X = 1 - \exp[-2O_v^B \int_0^{Gt} (1 - \exp(-Y^e))\, dy] \qquad (1)$$

$$\text{where: } Y^e = \frac{\pi I_B}{3} G^2 t^3 \left[1 - \frac{3y^2}{G^2t^2} + \frac{2y^3}{G^3t^3}\right] \quad (\text{if } t > y/G)$$

$$Y^e = 0 \quad (\text{if } t < y/G)$$

where G is the linear rate of growth of hydration product in any direction, O_v^B is the surface area of the C_3S particles per unit paste (sample) volume, and I_B is the nucleation rate per unit area of untransformed particle surface. Note that y (units of distance) disappears during the integration.

The kinetics of a boundary nucleation process can be described by two rate constants, each with units of inverse time:[1]

$$k_B = (I_B O_v^B)^{1/4} G^{3/4}; \; k_G = O_v^B G \qquad (2)$$

Rate constant k_B describes the rate at which the C_3S particle surfaces become covered with hydration product, while k_G describes the rate at which the capillary pore space between the particles fills in with product. The general shape of the rate curve (transformation rate versus time) depends on the relative values of k_B and k_G. When $k_B \ll k_G$, the boundary nucleation process reduces to the Avrami process, which generates a nearly symmetric rate peak. When $k_B \gg k_G$ the rate curve is asymmetric, with a steep upward leading slope and a more gradual downward trailing slope.

When applying nucleation and growth equations to hydration data, it is generally necessary to use two additional parameters, A and t_0.[11] Thus, these are four-parameter fits. Parameter A is a multiplication factor that scales the measured rate of heat output to the fractional rate of transformation; the fitted value of A is proportional to the area under the fit curves in Figure 2. Parameter t_0 is a time constant that offsets the start of the

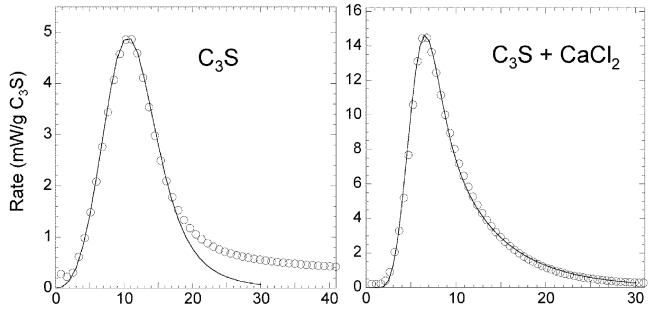

Figure 2. Boundary nucleation and growth fits to the measured rate data for pure C_3S paste (left) and $CaCl_2$-accelerated C_3S paste (right), both made with batch 1 C_3S and hydrated at 20 °C. Note the different scales. The open circles are the data, for which the experimental uncertainties are smaller than the circles, and the solid lines are the fits. For clarity, only a fraction of the calorimetry data are shown. The different quality of the model fits for the two pastes is discussed in the text.

nucleation and growth process from the time of mixing. The nucleation and growth equations are derived assuming that there are zero nuclei present at the time of mixing and that nucleation begins at a constant rate I_B at that time, and if this is the case then t_0 will be zero. If the nucleation rate is faster at the start of the reaction or if some nuclei have already formed by the time of mixing, then the fitted value of t_0 will be negative. If the nucleation rate is slower at the start of the reaction, or if nucleation is inhibited initially (a true induction period), then t_0 will be positive. A true induction period, defined as a time period when no nuclei are forming or growing, is not believed to occur for C_3S hydration in the absence of chemical admixtures.[5,12]

Both the Avrami and boundary nucleation models were fit to the calorimetry data. However, for the $CaCl_2$-accelerated pastes the Avrami model provided very poor fits that did not match the data past the peak in the hydration rate. Therefore, only the boundary nucleation fits are discussed here. The boundary nucleation fits to the calorimetry data shown in Figure 1 are presented in Figure 2. For the pure C_3S paste (Figure 2, left), the fit is quite good for the main hydration peak but deviates thereafter, in agreement with the previous study.[1] In contrast, for the $CaCl_2$-accelerated paste (Figure 2, right) the boundary nucleation fit continues to match the data closely as the hydration rate falls to a very low level.

The rather sharp transition from the downslope of the main hydration peak to a more slowly declining rate exhibited by the C_3S paste (but not by the $CaCl_2$-accelerated paste) has long been attributed[13] to a shift from nucleation and growth rate control to a diffusion-controlled reaction, where the time required for reactants to diffuse through a continuous layer of hydration product becomes rate controlling. With this hypothesis, the present results would indicate that in the presence of $CaCl_2$ the hydration process does not enter diffusion controlled kinetics during the early rapid hydration stage but continues to follow boundary nucleation and growth kinetics to a later stage of the reaction. Here, an alternative explanation for the transition observed in the pure C_3S paste will be proposed, based on the packing density of the C−S−H gel particles, that provides a better explanation of the experimental observations from both calorimetry and the SANS results presented in the next section.

The values of the fitted parameters for both batches of C_3S at 20 °C are given in Table 1, and the values for batch 2 C_3S at different temperatures are given in Table 2. The higher values of A obtained for batch 1 C_3S can be attributed to the higher specific surface area of this powder, which allows a greater amount of hydration product to form within a layer of a given thickness. For a given temperature and C_3S batch, parameter A is always more than twice as large for the $CaCl_2$-accelerated paste than for the C_3S control, indicating that significantly more hydration occurs by the boundary nucleation and growth process in the presence of $CaCl_2$. On the basis of an enthalpy of reaction for C_3S hydration of −121 kJ/mol,[14] for batch 1 C_3S the values of A correspond to overall degrees of hydration of about 36% for the control paste and about 78% for the accelerated paste.

From Table 1 it can also be seen that the values of rate constant k_B at 20 °C are about twice as high in the accelerated pastes as in the control pastes, while the values of rate constant k_G are roughly equal in the accelerated and control pastes. The larger value of the ratio k_B/k_G for the $CaCl_2$-accelerated pastes indicates a greater deviation of the kinetics from an Avrami-type process, providing an explanation for the observation made both here and elsewhere[15] that the Avrami equation provides a noticeably worse fit to $CaCl_2$-accelerated kinetics compared to pure C_3S kinetics. These findings are in good qualitative agreement with those of Peterson and Juenger,[7] who measured the cumulative amount of water bound into hydration products over time using quasielastic neutron scattering. Using a standard Avrami-type equation to fit their data, they found that the fitted values of parameter A and the single Avrami rate constant were about twice as high in the accelerated paste as in the control paste.

Previous analysis of a different batch of C_3S using isothermal calorimetry[1] found that the time constant t_0 was zero, whereas in the present study the time constants for pure C_3S hydration are negative. In another recent study,[16] the boundary nucleation model was successfully applied to C_3S hydration data obtained from quasielastic neutron scattering measurements, a technique that monitors the conversion of liquid water into bound water in the hydration products, resulting in a slightly negative time constant. We hypothesize that these discrepancies arise from exposure of the C_3S powder to moisture in the air during storage, which allows some C−S−H nuclei to form prior to mixing, resulting in a negative time constant. For the accelerated pastes in the present study, the t_0 values are consistently more positive than their corresponding controls. This is in agreement with previous observations[17] that $CaCl_2$ does not accelerate the very early hydration rate, prior to the onset of the main hydration peak, or shorten the time for calcium hydroxide to first precipitate. By increasing the calcium concentration in the pore solution, $CaCl_2$ may slow the initial rate of dissolution of the C_3S, which would delay the onset of rapid nucleation and growth by slowing the formation of a metastable layer of product within which nucleation occurs.

An advantage of the boundary nucleation growth fits is that they can be used to derive values of specific physical parameters associated with hydration. As can be seen from eq 2, if any one of the three parameters G, O_v^B, and I_B can be determined independently, then the other two can be calculated from the fitted values of the rate constants. The surface area parameter, O_v^B, can be calculated from the measured specific surface area of the powder and the estimated volume occupied by the hydration products when hydration is complete.[1] The derived values are $O_v^B = (1.07 \pm 0.08)\ \mu m^{-1}$ for batch 1 and $O_v^B = (0.71 \pm 0.06)\ \mu m^{-1}$ for batch 2. The resulting values of G and I_B are also listed in Tables 1 and 2.

The values of the linear growth rate, G, are similar in all the pastes tested at 20 °C (Table 1), and the values are in good agreement with the value of 0.081 $\mu m\ h^{-1}$ previously obtained

TABLE 1: Boundary Nucleation and Growth Fit Parameters A, t_0, k_B, and k_G for Hydration at 20°C, Together with Derived Physical Parameters G and I_B (See Eq 2[a])

	A (kJ/mol)	t_0 (h)	k_B (h^{-1})	k_G (h^{-1})	G^b	$I_B{}^c$
$C_3S(1)$	42 (2)[d]	−0.5 (2)	0.081 (3)	0.096 (4)	0.090 (5)	0.057 (3)
$C_3S(1) + CaCl_2$	92 (4)	1.4 (2)	0.162 (6)	0.075 (3)	0.070 (4)	1.84 (11)
$C_3S(2)$	31 (1)	−2.3 (2)	0.068 (3)	0.051 (2)	0.072 (4)	0.078 (5)
$C_3S(2) + CaCl_2$	78 (3)	0.0 (2)	0.122 (5)	0.053 (2)	0.075 (4)	0.75 (5)

[a] Values of the surface area parameter (calculated independently) are $O_v^B = 1.07\ \mu m^{-1}$ for $C_3S(1)$ and $O_v^B = 0.71\ \mu m^{-1}$ for $C_3S(2)$. [b] Units of ($\mu m\ h^{-1}$). [c] Units of ($\mu m^{-2}\ h^{-1}$). [d] The numbers in parentheses are estimated standard deviations in least significant digits.

TABLE 2: Boundary Nucleation and Growth Fit Parameters A, t_0, k_B, and k_G for Hydration of Batch 2 C_3S at Different Temperatures, Together with Derived Physical Parameters G and I_B

	A (kJ/mol)	t_0 (h)	k_B (h^{-1})	k_G (h^{-1})	G^a	$I_B{}^b$
H_2O (10 °C)	42 (2)[c]	−3.6 (2)	0.033 (1)	0.031 (1)	0.044 (2)	0.020 (1)
H_2O (20 °C)	31 (1)	−2.3 (2)	0.068 (3)	0.051 (2)	0.072 (4)	0.078 (5)
H_2O (30 °C)	24 (1)	−1.8 (2)	0.118 (5)	0.079 (3)	0.111 (7)	0.20 (1)
H_2O (40 °C)	23 (1)	−1.4 (2)	0.185 (7)	0.116 (5)	0.163 (9)	0.38 (2)
$CaCl_2$ (10 °C)	83 (3)	−0.2 (2)	0.055 (2)	0.025 (1)	0.035 (2)	0.31 (2)
$CaCl_2$ (20 °C)	78 (3)	0.0 (2)	0.122 (5)	0.053 (2)	0.075 (4)	0.75 (5)
$CaCl_2$ (30 °C)	68 (3)	0.1 (2)	0.235 (9)	0.105 (4)	0.148 (8)	1.33 (8)
$CaCl_2$ (40 °C)	59 (2)	0.0 (2)	0.41 (2)	0.194 (8)	0.27 (2)	1.90 (11)

[a] Units of ($\mu m\ h^{-1}$). [b] Units of ($\mu m^{-2}\ h^{-1}$). [c] The numbers in parentheses are estimated standard deviations in least significant digits.

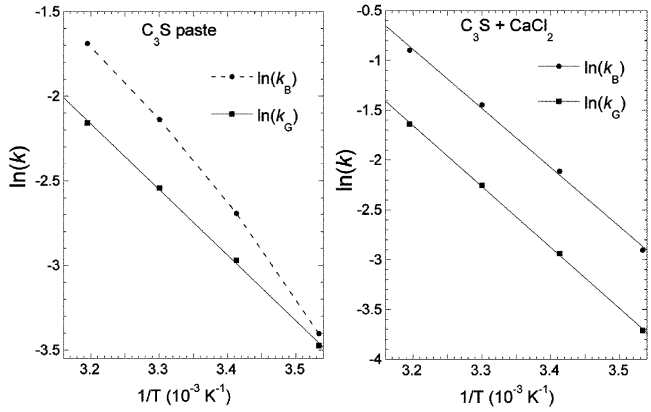

Figure 3. Arrhenius plots of the rate constants k_B and k_G for pure C_3S paste (left) and $CaCl_2$-accelerated C_3S paste (right), made with batch 2 C_3S. The solid lines are straight-line fits, from which activation energies can be calculated (see text). The dashed line for k_B in the left panel is a guide to the eye.

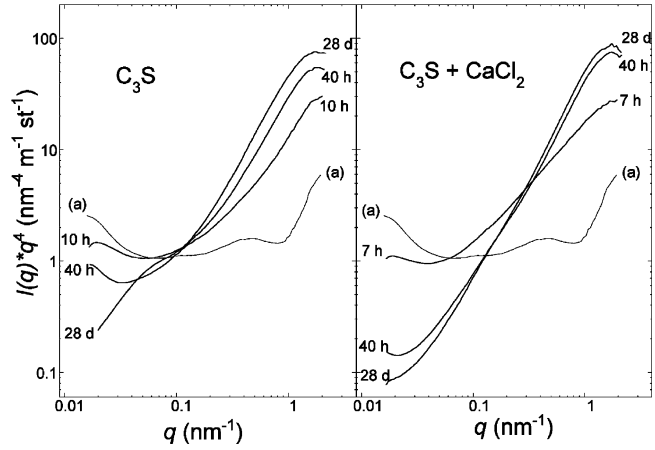

Figure 4. Absolute calibrated SANS data for hydrating C_3S control paste (left) and for $CaCl_2$-accelerated C_3S paste (right). Data set (a) represents the scattering from the anhydrous powder in both plots. The first data set from each hydrating paste (10 h for C_3S and 7 h for $C_3S + CaCl_2$) is close to the time of the hydration rate peak as measured by calorimetry.

for pure C_3S paste following the same procedure.[1] The linear growth rate has also been estimated from direct observations of the formation of C−S−H product on a flat, polished C_3S surface using atomic force microscopy.[18] The latter measurements yielded values of 0.065 $\mu m\ h^{-1}$ parallel to the surface and 0.148 $\mu m\ h^{-1}$ perpendicular to the surface. Given the significant differences in both the starting conditions (i.e., fine powder vs flat surface) and in the method of determining G, the agreement with the present results is quite good.

The values of the nucleation rate I_B obtained from the fits at a given temperature are significantly higher in the accelerated pastes, by a factor of ≈ 30 for batch 1 and ≈ 9 for batch 2. Since the values of the other two fundamental kinetic parameters are similar (for G) or identical (for O_v^B) with and without $CaCl_2$, the significantly accelerated hydration kinetics (in particular the much steeper slope of the rate curve leading up to the hydration peak and the higher value of the peak rate) can be specifically attributed to a significantly higher nucleation rate that leads to more regions of hydration product growing at the same time.

Figure 3 shows Arrhenius plots (ln k versus $1/T$) for the fitted rate constants from hydration of batch 2 C_3S. For the pure C_3S paste, the plot for k_G is linear across the full temperature range, and the resulting activation energy is (32.2 ± 1.2) kJ/mol. The plot for k_B is not linear, but has a slope that decreases with temperature. These results are in agreement with previous boundary nucleation and growth fits for pure C_3S paste.[1] For the $C_3S + CaCl_2$ paste, the activation energies are higher: (49.3 ± 2.0) kJ/mol for k_B and (50.8 ± 2.0) kJ/mol for k_G. These values are in good agreement with the value of 49.4 kJ/mol reported for the same system by Vollet and Craievich[15] based on Avrami fits to changes in small-angle X-ray scattering data. Because k_G depends linearly on the growth rate and on the temperature-invariant particle surface area (see eq 2), the activation energies reported above for k_G also apply to the product growth rate, G.

Microstructure Development Measured by SANS. Absolute calibrated SANS data across the full q-range for both types of paste at different times are shown in Figure 4. Data set (a) is the anhydrous C_3S powder; this data set was normalized to the paste data to account for the mass of C_3S in the beam and the different scattering intensity when the pore space is filled with air rather than water. The size of the features that can

contribute to the observed scattering is inversely proportional to q. The normalized scattering intensity, $I(q)$, tends to decrease rapidly with increasing q. However, in Figure 4 $I(q)q^4$ is plotted instead of $I(q)$, and this generally increases with q. This type of plot has the advantage of emphasizing differences between related data sets.

For data set (a), the essentially constant value of $I(q)q^4$ at intermediate q values represents Porod scattering that can be used to calculate the powder surface area. The increase in $I(q)q^4$ at high q for data set (a) has been observed previously[19] and can be attributed to the presence of a small amount of hydration product on the powder surface due to contact with moisture in the air. In Figure 4 it can be seen that over the first several hours of hydration the intensity at higher q values increases with time, as hydration product, particularly C−S−H gel with a nanoscale structure, grows into the pore space between the particles. A brief Porod scattering range at the highest q-values reflects the surface area of the C−S−H gel hydration product and can be used to calculate the specific surface area of the hydrating pastes, as discussed below. The intensity in the low-q regime decreases with hydration time, as Porod scattering from the sharp interface between the C_3S particles and the pore fluid is softened by the presence of an intervening layer of hydration product, and as the C_3S particles are consumed by hydration. The plots in Figure 4 indicate that for the pure C_3S paste significant scattering originating from the C_3S particles remains after 28 days of hydration, while for the $CaCl_2$-accelerated paste this scattering essentially disappears by 40 h of hydration from the q-range measured by this instrument.

More specific and quantitative insights into the kinetics of microstructure development can be obtained by applying various microstructural models to the SANS data and then analyzing the changes in the resulting parameters with hydration time. However, to properly compare the C_3S and $C_3S + CaCl_2$ pastes, it is necessary to know the relevant neutron scattering contrast $\Delta\rho^2 = (\rho_{solid} - \rho_{H_2O})^2$ for each paste type, where ρ_{solid} and ρ_{H_2O} are the neutron scattering length densities of the hydration product and of the pore water, respectively. For cement-based materials the fine structure, and thus the value of ρ_{solid}, is dominated by the C−S−H gel phase. For phases with well-defined composition and mass density such as water, the value of ρ can be calculated directly ($\rho_{H_2O} = -0.561 \times 10^{14}$ m^{-2}). However, a key aspect of C−S−H gel is its incorporation of H_2O, which occurs as chemically bound OH^- groups, physically adsorbed water, and liquid water in gel pores. This complicates the definition of the solid phase composition and density.

Recently, the authors developed a small-angle scattering based method to accurately determine the value of ρ_{solid} in a cement paste, as well as the composition and mass density of the solid C−S−H nanoparticles, by performing deuterated fluid exchange using both H_2O/D_2O and CH_3OH/CD_3OH.[20] The analysis also yields information about the nanoscale distribution of $Ca(OH)_2$, another hydration product. Results for C_3S paste with estimated standard deviation uncertainties, previously published,[20] are $\rho_{solid} = (2.560 \pm 0.005) \times 10^{14}$ m^{-2}, $C_{1.7}-S-H_{1.80}$, $d = (2.604 \pm 0.022)$ Mg/m^3). Because of the possibility that $CaCl_2$ changes the basic composition and density of the solid C−S−H that forms in the paste, this procedure was repeated using 28-day old $CaCl_2$-accelerated paste made with batch 1 C_3S. The results ($\rho_{solid} = (2.59 \pm 0.02) \times 10^{14}$ m^{-2}, $C_{1.7}-S-H_{1.75}$, $d = (2.620 \pm 0.02)$ Mg/m^3) are quite similar. This indicates that the differences in nanostructure caused by $CaCl_2$ (e.g., Figure 4) are associated with differences in the arrangement and possibly the shape of the C−S−H nanoparticles, rather than their intrinsic composition.

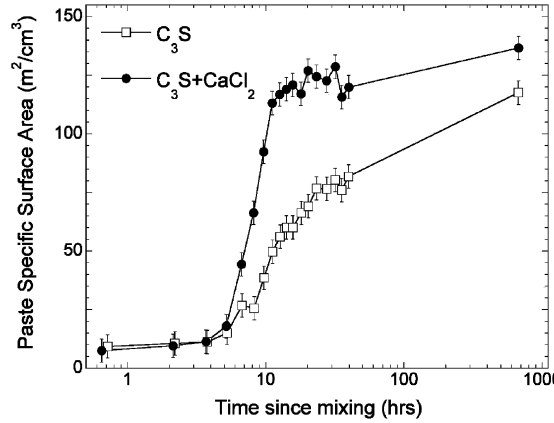

Figure 5. The paste specific surface area, S_T, determined from the high-q SANS data as a function of time, for pure C_3S and $CaCl_2$-accelerated pastes. The surface area values are normalized to the volume of the specimen. Vertical bars are estimated uncertainties.

The specific surface area of a hydrated paste per unit specimen volume, S_T, can be determined from the Porod scattering at the highest accessible q-values above $q = 1.4$ nm^{-1}:

$$S_T = C_P/2\pi\Delta\rho^2 \tag{3}$$

where C_P is the constant of proportionality for the Porod scattering at high q. Figure 5 shows S_T as a function of time for both hydrating pastes. The kinetics of surface area development are similar in nature to the kinetics of the total heat evolution (see Figure 1 inset), confirming that $CaCl_2$ stimulates the formation of a greater amount of C−S−H hydration product at a given time during the early hydration period.

Additional parameters related to the microstructure development of these pastes can be obtained by applying a previously developed fractal microstructure model[4,21−23] to the SANS data over almost the entire accessible q-range. The model describes three separate scattering regimes present in the data. At low q-values surface fractal scattering is generated from the deposition of hydration product onto the hydrating cement grains. This is modeled by a fractal scaling exponent (D_s), an upper limit length scale, or correlation length (ξ_s), and the smooth surface area (ignoring fractal roughness) of the cement particles S_0. At intermediate q-values, volume fractal scattering arises from the random aggregations of the basic C−S−H nanoparticles, and this is the most prominent scattering regime in well-hydrated pastes. This is modeled by another fractal exponent and correlation length (D_v and ξ_v) along with the volume fraction of solid nanoscale product, ϕ_{CSH}. At high q-values, just below the Porod regime, single particle scattering applies, allowing the size (a_s) and local packing fraction (η) of the C−S−H building block particles to be determined. A constant background term is also used to refine the previously performed flat background subtraction. While the total number of adjustable parameters is large, the scale separation between the three scattering regimes described above means that only a small subset of these parameters are used to fit the data in each regime. More details on the model and its application are given in the above citations.

Good fits to the SANS data over two decades of scattering vector and nearly six decades of intensity for hydration times ranging from 8 to 40 h were obtained with the model described

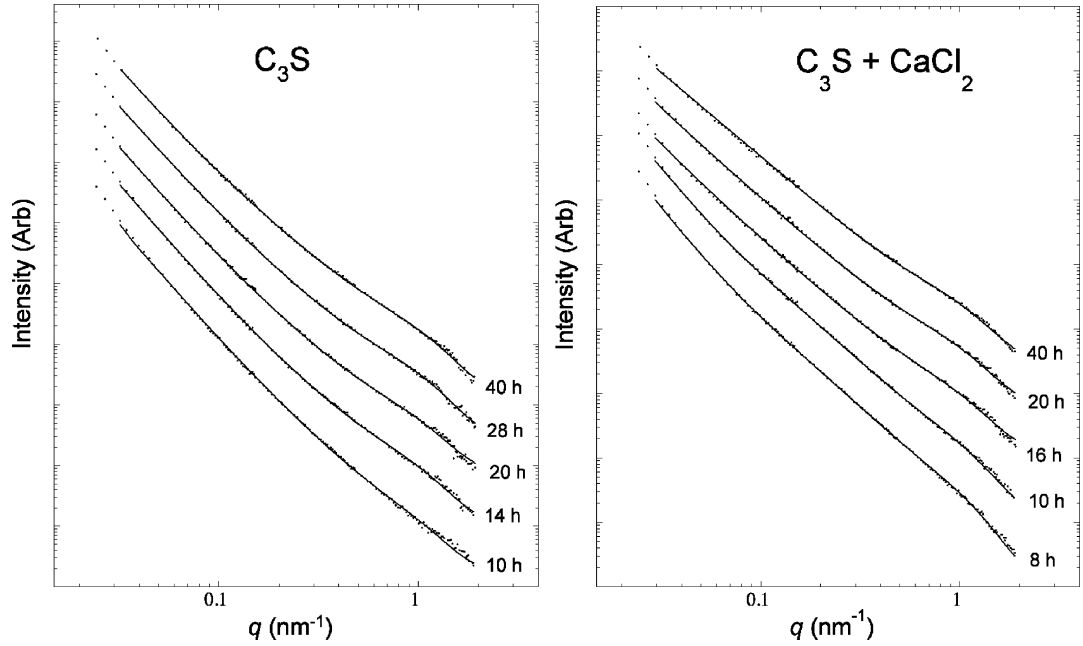

Figure 6. SANS data for hydrating C_3S control paste (left) and for $CaCl_2$-accelerated C_3S paste (right). The lines are fits obtained with the fractal microstructure model described in the text. Data sets are offset for clarity. The experimental uncertainties are indicated by the scatter in the data.

above (see Figure 6). At earlier hydration times poor statistics in the data prevented unique fits from being obtained. Interestingly, for the $C_3S + CaCl_2$ paste the fitted contribution from surface fractal scattering drops to zero after about 25 h of hydration. Thus, after this time data from this paste are fitted only by volume fractal scattering over all but the highest q-values.

The values of the primary gel particle diameter and volume fractal exponent did not exhibit statistically significant changes with hydration time, and the average values were similar in the C_3S paste ($a_s = 4.26 \pm 0.03$ nm, $D_v = 2.55 \pm 0.03$) and the $C_3S + CaCl_2$ paste ($a_s = 4.21 \pm 0.05$ nm, $D_v = 2.52 \pm 0.04$). These are in good agreement with previously published values[21,23] for portland cement pastes of various ages. The surface fractal exponent and associated correlation length could not be determined as accurately as they show a high degree of covariance and the fit quality is not highly sensitive to their values, particularly for ξ_s. Values of D_s were in the range of 2.1−2.3 and ξ_s values were in the range of 1−2 μm.

The three parameters of greatest interest for this study, ϕ_{CSH}, S_0, and ξ_v, are plotted in Figure 7. At left, the values are plotted as a function of time, while at right the same values are plotted as a function of the degree of hydration, which is calculated from the calorimetry data conducted on the same C_3S powder at the same temperature (20 °C). In the latter plots, data from the 28-day old C_3S paste is also included, using a degree of hydration value of 0.85 extrapolated from the measured heat of hydration.

The volume fraction of solid material in the volume fractal component, ϕ_{CSH}, increases with hydration time, as expected (Figure 7, top left). As with the development of surface area and the evolution of heat, the values increase more quickly and reach higher values for the accelerated paste. When plotted as a function of degree of hydration (Figure 7, top right), the ϕ_{CSH} values from the two pastes appear to fall on a single curve, indicating that at a given degree of hydration, the amount of nanoscale solid product detected by SANS is not affected by the presence of $CaCl_2$.

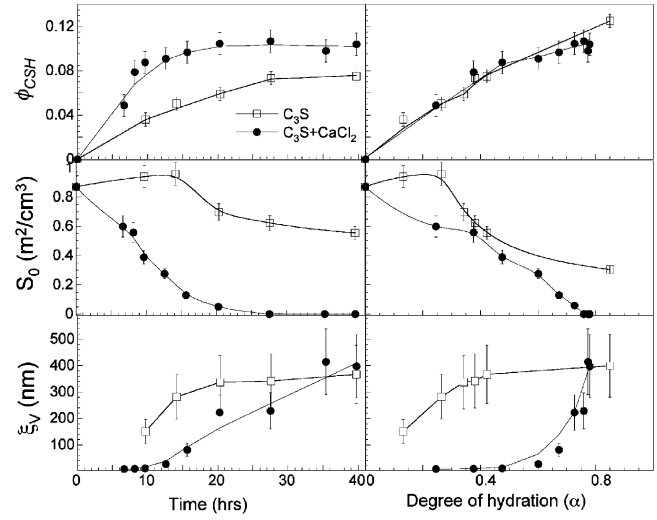

Figure 7. Fitted values of the volume fraction of nanoscale solid, ϕ_{CSH}, the fractally smooth surface area associated with the hydrating C_3S particles, S_0, and the correlation length for volume fractal scaling, ξ_v, for C_3S paste (open symbols) and $C_3S + CaCl_2$ paste (solid symbols). At left the values are plotted as a function of hydration time. At right the same values are plotted as a function of the fractional degree of hydration. The vertical bars are estimated uncertainties and the lines are guides to the eye.

The smooth surface area S_0, which represents scattering from the original cement particles, shows very different behavior in the two pastes (Figure 7, middle). The initial value of S_0 in both pastes is taken as the surface area of the anhydrous powder, normalized appropriately to the paste specimens. In the pure C_3S paste, S_0 first remains level or increases slightly during the early rapid hydration period, and then decreases gradually thereafter to roughly half its initial value. In the accelerated paste, S_0 decreases sharply with hydration time, reaching zero after about 25 h of hydration. When plotted against degree of hydration, the value of S_0 decreases at an approximately linear rate. The loss of surface fractal scattering induced by $CaCl_2$

was previously reported for portland cement paste specimens made with and without $CaCl_2$ and analyzed at the age of 28 days.[4]

Very different behavior is exhibited by the correlation length for volume fractal scattering, ξ_v (Figure 7, bottom). For the C_3S paste the value of ξ_v increases gradually with time and degree of hydration, in qualitative agreement with previous results for portland cement.[21] For the $CaCl_2$-accelerated paste, the values of ξ_v are significantly lower at low degrees of hydration (~10 nm) and then increase by over an order of magnitude with time and degree of hydration, eventually reaching similar values as in the pure C_3S paste. The behavior of the parameters S_0 and ξ_v is evidence of fundamental differences in the hydration process that are independent of the obvious kinetic (accelerating) effects of $CaCl_2$.

Discussion

Taken together, the analysis of the calorimetry and SANS measurements allows a more complete description of the hydration process with and without $CaCl_2$ to be developed. In many ways, the hydration of the $CaCl_2$-accelerated C_3S paste is the more straightforward to interpret. The hydration rate measured by calorimetry closely follows boundary nucleation and growth kinetics throughout the first 30 h of hydration, and perhaps beyond, as the degree of hydration reaches close to 80% and the hydration rate drops to near zero. It is thus reasonable to assume that the basic assumptions of the boundary nucleation process hold in this case: hydration product nucleates at the particle surfaces and grows outward at a constant rate in all directions, and the overall rate first increases as the number and size of the regions of hydration product increase, and then decreases as regions of product impinge, halting further growth along their common interface. Impingement occurs first between regions nucleated on the same particle, and then later between product layers formed on adjacent particles.

The SANS data from the $CaCl_2$-accelerated paste support this interpretation. As hydration proceeds, the high-q scattering associated with nanoscale hydration product increases, while the scattering at lower-q values associated with the surface of the original C_3S particles decreases and essentially disappears. Thus, hydration with $CaCl_2$ can be interpreted as a relatively simple process of the C_3S particles dissolving to form nanoscale hydration product that occupies both the original pore space and the volume originally occupied by the particles. The average correlation length for volume fractal scaling, ξ_v, is small at early times (corresponding to the upslope of the main calorimetry rate peak) when many new regions of hydration product are forming and the average size of the individual regions is small. Parameter ξ_v then increases at later times (corresponding to the downslope of the rate peak) as the average size of hydration product regions increases through growth and impingement.

The pure C_3S paste exhibits some important differences from the above scenario. The nucleation rate as determined from the boundary nucleation fits is significantly lower than in the $CaCl_2$-accelerated paste, leading to a less steep upslope on the main rate peak. This difference can be attributed to the absence of the chemical effect of the $CaCl_2$ in the solution. The measured kinetics can be fitted closely with the boundary nucleation model through the main hydration peak, but unlike the $CaCl_2$-accelerated paste, the measured and fitted rates deviate as the measured rate transitions rather sharply from a steep downslope to a more gradual decrease (see Figure 2). In addition, the total amount of hydration occurring by boundary nucleation and growth, as measured by the fitted value of parameter A, is much smaller in the pure C_3S paste. We assert that this last point provides an important clue as to the differences in the hydration process introduced by $CaCl_2$.

The end of the nucleation and growth reaction regime occurs when the volume available for the process is filled with the product phase. In a hydrating paste, the total volume available for product at a given time consists of the original water-filled space plus the space formerly occupied by dissolved particles, which is determined primarily by the water/cement mass ratio (w/c). However, calorimetry measurements of pastes made with the same C_3S powder mixed at different w/c indicate that the hydration kinetics are essentially independent of the w/c.[1] Therefore, it is hypothesized that during the early nucleation and growth period hydration product forms only within a reaction volume that extends a fixed distance away from the surface of the particles. In this case, the volume available for product will depend primarily on the powder surface area rather than the w/c. This is supported by hydration experiments[24] on pastes made from C_3S powders with different average particle sizes, all mixed at the same w/c: the amount of hydration occurring during nucleation and growth (parameter A) increases significantly as the particle size decreases.[24] In the present paper, all pastes are made with the same w/c, and for a given paste type (with or without $CaCl_2$), the powder with a modestly higher surface area (C_3S batch 1) gives a slightly larger value of A, in agreement with this hypothesis.

Therefore, the much smaller fitted value of A in the pure C_3S pastes indicates that the available reaction volume is being filled at a much lower degree of hydration as compared to the $CaCl_2$-accelerated pastes. There are two possibilities: the reaction volume could be increased in the presence of $CaCl_2$ or the bulk density of the hydration product, including internal gel porosity, is increased by $CaCl_2$ so that more solid hydration product fits into the same volume. The present results, taken together, support the latter mechanism; specifically, a difference in the packing density of the C−S−H formed at early times in the two paste types. However, a difference in reaction volume is also possible.

The measured early hydration rate in the C_3S paste can be interpreted as follows. Hydration product with a large amount of internal porosity, and thus a low density, forms initially according to the boundary nucleation process, filling the available reaction volume at a relatively low degree of hydration. As the remaining volume available to the nucleation and growth process becomes limited, the formation of new product causes the existing product to densify. Thus, more hydration product is able to fit into the same amount of space. The latter process, which is not described by the boundary nucleation equations, explains the deviation between the measured rate and the fit. This hypothesis is supported by the behavior of ξ_v, which is much higher in the pure C_3S paste during the early stages of the hydration process as compared to the $CaCl_2$-accelerated paste. This suggests the formation of fewer regions of hydration product in the pure C_3S paste that grow quickly to a relatively large size.

On the basis of the assumption that the C−S−H gel is a nanogranular material consisting of randomly agglomerated solid particles, the differences in density implied by the present results indicate that the packing density is low initially and then increases with time, particularly in the C_3S paste. Because the surface area accessible to SANS is reduced by particle−particle contacts,[23] it follows that the measured specific surface area per mole of C−S−H should decrease as the packing density increases. The molar amount of C−S−H per unit paste volume

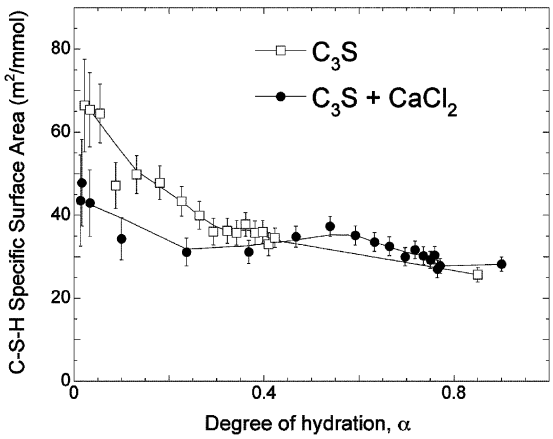

Figure 8. Surface area of the C−S−H gel phase as a function of the fractional degree of hydration. The degree of hydration at a given time was calculated by dividing the cumulative heat output measured by calorimetry by the theoretical heat output for complete C_3S hydration (121 kJ/mol). The amount of C−S−H at a given time was calculated from the degree of hydration assuming a fixed Ca/Si molar ratio of 1.7.

can be estimated from the w/c, the degree of hydration as determined from the heat evolution, and the Ca/Si ratio of the C−S−H, assumed to be fixed at 1.7. Dividing the SANS surface area per unit paste volume, S_T, by this value gives the molar surface area of the C−S−H phase as a function of degree of hydration, as shown in Figure 8. The surface area per mole of C−S−H decreases significantly with time during the early stages of hydration of the pure C_3S paste, and much less so for the $CaCl_2$-accelerated paste. In the later stages of hydration the values appear to converge on a constant value of about 27 m^2/mmol. Interestingly, recent simulations of the nucleation and growth hydration process of pure C_3S powder also indicate that the measured early hydration kinetics can be reproduced by assuming that the C−S−H phase becomes more densely packed with time.[25]

The tendency for the C−S−H phase to form with different morphologies is well established, for example, through microscopy studies showing distinct regions of inner product and outer product.[26] One of the authors has proposed a colloid model of C−S−H[27,28] that explains a wide variety of density and surface area data by proposing two packing densities of C−S−H in well-hydrated paste, referred to as high-density (HD) C−S−H and low-density (LD) C−S−H. Another study[29] showed that the C−S−H phase densifies slowly over time and more rapidly on drying and heat curing. The present study suggests that even lower densities are present during the first several hours of the hydration process, at least for pure C_3S pastes.

An important chemical effect of the addition of $CaCl_2$ is to increase the calcium concentration in solution during the early hydration period,[17] which is likely to directly affect the C−S−H gel formation process. Gaboriaud et al.[30,31] studied the rate of formation and colloidal structure of C−S−H phases formed by precipitation from various aqueous solutions containing silicon, calcium, and alkali species and found that the calcium concentration was the main factor controlling aggregation and gelation. At low calcium concentrations relatively large aggregations form initially which then densify slowly with time, whereas at higher calcium concentrations there is the rapid formation of a large number of smaller aggregates which can densify by cluster−cluster aggregation.[31] This is in good qualitative agreement with the SANS results for the first several hours of hydration, particularly the development of the volume fractal correlation length with time in the two types of paste (see Figure 7).

Another important difference in the two pastes analyzed here is the presence of surface fractal scattering associated with the original C_3S particles at all hydration times in the pure C_3S paste, and the decline of this scattering to undetectable levels in the $CaCl_2$-accelerated paste. According to a previous interpretation,[21] dense hydration product formed within the boundaries of the original cement grains generates surface fractal scattering from its overall outer surface. The present results suggest that this does not happen in the presence of $CaCl_2$. This is supported by a study[6] that used transmission soft X-ray microscopy to study the hydration of individual grains of C_3S suspended in solutions with and without $CaCl_2$. That study found that the hydration product formed in the presence of $CaCl_2$ appeared more uniform than that of a control specimen, with no visible distinction between inner and outer product.

An interesting implication of the present results is that the hydration reactions do not become diffusion controlled as early as is usually assumed. In the $CaCl_2$-accelerated paste, the agreement between the boundary nucleation fit and the calorimetry data remains good until almost 80% hydration, long past the point where a complete layer of hydration product has formed around the particles. With the present interpretation, the deviation from the fit with the C_3S paste occurs due to densification of the C−S−H as discussed above, so no firm conclusion about diffusion control past this point can be drawn. However, it seems reasonable to assume that the lower density product that forms in the pure C_3S paste should be at least as permeable as the product formed in the $CaCl_2$-accelerated paste. Given that cement hydration continues at a slow and declining rate for 28 days and beyond, and that the hydration product continues to densify, it does seem inevitable that the rate should become diffusion controlled at some point.

Conclusions

The addition of $CaCl_2$ to tricalcium silicate (C_3S) paste significantly increases both the early hydration rate and the total amount of early hydration, in agreement with previous findings. Application of the boundary nucleation model to the early hydration rate data obtained from isothermal calorimetry indicates that $CaCl_2$ significantly increases the rate of nucleation of hydration product on the surface of the C_3S particles but has relatively little effect on the product growth rate.

The nanostructural development in the pure C_3S and $CaCl_2$-accelerated pastes, measured using SANS, showed important differences. After a few hours of hydration, both types of paste developed two fractal scattering regimes previously identified as volume fractal scattering associated with nanoscale C−S−H gel formation and surface fractal scattering associated with the deposition of hydration product onto the initially smooth surfaces of the C_3S particles. In the pure C_3S paste the surface fractal scattering remains prominent throughout the hydration process, but in the $CaCl_2$-accelerated paste the surface fractal scattering rapidly declines in intensity and essentially disappears by the age of 1 d.

A SANS-based method involving deuterated fluid exchange was used to measure the composition and mass density of the solid C−S−H nanoparticles in 28-day old $CaCl_2$-accelerated paste. The results, with estimated standard deviation uncertainties, are ($\rho_{solid} = (2.59 \pm 0.02) \times 10^{14}$ m^{-2}, $C_{1.7}$−S−$H_{1.75}$, $d = (2.620 \pm 0.02)$ Mg/m^3). These are similar to previously obtained results for pure C_3S paste, indicating that differences in nanostructure caused by $CaCl_2$ are associated with differences in the arrangement and possibly the shape of the C−S−H nanoparticles, rather than their intrinsic composition.

A description of the hydration process that explains the key observations was developed. In the pure C_3S paste, C−S−H hydration product formed by nucleation and growth develops initially with a large amount of internal porosity. As the available reaction volume becomes filled, additional hydration causes the C−S−H to become more tightly packed, allowing more solid product to fit into the same space. This process violates the assumptions of the nucleation and growth model, causing a deviation between the calorimetry data and the fit. In the $CaCl_2$-accelerated paste, the internal porosity does not vary significantly with time, possibly due to the significantly higher rate of nucleation of new regions of C−S−H. As a result, the boundary nucleation and growth model is able to reproduce the measured hydration kinetics throughout the early hydration process. This is also supported by the variation in the specific surface area of the C−S−H gel with time, determined here by combining the SANS and calorimetry data from parallel pastes. In the C_3S paste the surface area per mole of C−S−H decreases significantly with time, consistent with a decrease in its internal porosity, while for the $CaCl_2$-accelerated paste this parameter is relatively constant with time. The value of the C−S−H specific surface area measured by SANS (27 m^2/mmol) is similar in both pastes after 28 days of hydration.

Acknowledgment. This work utilized neutron scattering facilities supported in part by the National Science Foundation under Agreement No. DMR-0454672.

References and Notes

(1) Thomas, J. J. *J. Am. Ceram. Soc.* **2007**, *90*, 3282.
(2) Thomas, J. J.; Jennings, H. M.; Chen, J. J. *J. Phys. Chem. C* **2009**, *113*, 4327.
(3) Allen, A. J. *J. Am. Ceram. Soc.* **2005**, *88*, 1367.
(4) Allen, A. J.; Thomas, J. J. *Cem. Concr. Res.* **2007**, *37*, 319.
(5) Taylor, H. F. W., *Cement Chemistry*, 2nd ed.; Thomas Telford: London, 1997.
(6) Juenger, M. C. G.; Monteiro, P. J. M.; Gartner, E. M.; Denbeaux, G. P. *Cem. Concr. Res.* **2005**, *35*, 19.
(7) Peterson, V. K.; Juenger, M. C. G. *Chem. Mater.* **2006**, *18*, 5798.
(8) Glinka, C. J.; Barker, J. G.; Hammouda, B.; Kreuger, S.; Moyer, J. J.; Orts, W. J. *J. Appl. Crystallogr.* **1998**, *31*, 430.
(9) Garrault, S.; Nonat, A. *Langmuir* **2001**, *17*, 8131.
(10) Cahn, J. W. *Acta Met.* **1956**, *4*, 449.
(11) Thomas, J. J.; Jennings, H. M. *Chem. Mater.* **1999**, *11*, 1907.
(12) Gartner, E. M.; Gaidis, J. M. Hydration Mechanisms, I. In *Materials Science of Concrete*; Skalny, J. P., Ed.; The American Ceramic Society: Westerville, OH, 1989.
(13) Kondo, R.; Ueda, S. In Kinetics and Mechansms of the Hydration of Cements, Proceedings of the Fifth International Symposium on the Chemistry of Cements, Tokyo, 1968; Tokyo, 1968; p 203.
(14) Gartner, E. M.; Young, J. F.; Damidot, D. A.; Jawed, I., Hydration of Portland Cement. In *Structure and Performance of Cements*; Barnes, P., Bensted, J., Eds. Spon Press: London, 2002; Chapter 3.
(15) Vollet, D. R.; Craievich, A. F. *J. Phys. Chem. B* **2000**, *104*, 12143.
(16) Peterson, V. K.; Whitten, A. E. *J. Phys. Chem. C* **2009**, *113*, 2347.
(17) Brown, P. W.; Harner, C. L.; Prosen, E. J. *Cem. Concr. Res.* **1985**, *16*, 17.
(18) Garrault, S.; Finot, E.; Lesniewska, E.; Nonat, A. *Mater. Struct.* **2005**, *38*, 435.
(19) Allen, A. J.; Oberthur, R. C.; Pearson, D.; Schofield, P.; Wilding, C. R. *Philos. Mag. B* **1987**, *56*, 263.
(20) Allen, A. J.; Thomas, J. J.; Jennings, H. M. *Nat. Mater.* **2007**, *6*, 311.
(21) Allen, A. J. *J. Appl. Crystallogr.* **1991**, *24*, 624.
(22) Allen, A. J.; Livingston, R. A. *Advn. Cem. Based Mater.* **1998**, *8*, 118.
(23) Thomas, J. J.; Allen, A. J.; Jennings, H. M. *J. Am. Ceram. Soc.* **2008**, *91*, 3362.
(24) Allen, A. J.; McLaughlin, J. C.; Neumann, D. A.; Livingston, R. A. *J. Mater. Res.* **2004**, *19*, 3242.
(25) Bishnoi, S.; Scrivener, K. L. *Cem. Concr. Res.* **2009**, *39*, 849.
(26) Richardson, I. G. *Cem. Concr. Res.* **2004**, *34*, 1733.
(27) Jennings, H. M. *Cem. Concr. Res.* **2000**, *30*, 101.
(28) Jennings, H. M. *Cem. Concr. Res.* **2008**, *38*, 275.
(29) Jennings, H. M.; Thomas, J. J.; Gevrenov, J. S.; Constantinides, G.; Ulm, F.-J. *Cem. Concr. Res.* **2007**, *37*, 329.
(30) Gaboriaud, F.; Nonat, A.; Chaumont, D.; Craievich, A. *J. Phys. Chem. B* **1999**, *103*, 5775.
(31) Gaboriaud, F.; Nonat, A.; Chaumont, D.; Craievich, A. *J. Colloid Interface Sci.* **2002**, *253*, 140.

JP907078U